Investigating the Ice Water Path in Convective Cloud Life Cycles to Improve Passive Microwave Rainfall Retrievals

RAMON CAMPOS BRAGA AND DANIEL ALEJANDRO VILA

Satellite and Environmental Systems Division, Center for Weather Forecast and Climate Studies, National Institute for Space Research, São Paulo, Brazil

(Manuscript received 18 December 2013, in final form 25 April 2014)

ABSTRACT

This study focuses on the possible relationship between ice water path (IWP) retrievals using high-frequency channels (89 and 150 GHz) from the Advanced Microwave Sounding Unit-B and Moisture Humidity Sounder sensors (*NOAA-16–NOAA-19*) and the life cycle stage of convective clouds. In the first part of this study, the relationship between IWP and the cloud area expansion rate is analyzed using the 235-K isotherm from *Geostationary Operational Environmental Satellite-12* (*GOES-12*) thermal infrared images (10.7 μm). Next, the relationships between cloud convective fraction, rain rates (from ground radar), and cloud life cycle are analyzed. The selected area and time period coincide with the research activities of the Cloud Processes of the Main Precipitation Systems in Brazil: A Contribution to Cloud Resolving Modeling and to the Global Precipitation Measurement (CHUVA)–Geostationary Lightning Mapper (GLM) project at São José dos Campos, Brazil. The results show that 84% of precipitating clouds contain ice, according to the Microwave Surface and Precipitation Products System (MSPPS) algorithm. Convective systems in the intensifying stage (when the area is expanding and the minimum temperature is decreasing) tend to have larger IWPs than systems in the dissipating stage. Larger rain rates and convective fractions are also observed from radar retrievals in the early stage of convection compared with mature systems. Hydrometeor retrieval data from polarimetric X-band radar suggest that particle effective diameter D_e and IWP patterns inferred with the MSPPS algorithm could be used to determine the life cycle stage of a given convective system. Using this information, a new set of equations is evaluated for rainfall retrievals using D_e and IWP from the current retrieval algorithm. This new approach outperforms the current algorithm in the studied region.

1. Introduction

Ice clouds play a significant role in the atmospheric radiation budget and have a large effect on weather and climate forecasts (Rossow and Schiffer 1991, 1999). Different methods have been adopted to estimate the ice water path (IWP) in clouds containing ice. For thin ice clouds, for example, cirrus, IWP retrievals are reasonably accurate using infrared (IR) information. Moreover, for thick ice clouds, IWP retrievals using passive microwave information have been used to obtain better results (Vivekanandan et al. 1991; Sun and Weng 2012).

Here, IWP is calculated as a function of ice particle diameter D_e, viewing angle θ, and particle density ρ using passive microwave sensors (Liu and Curry 1998; Weng and Grody 2000). For convective clouds with relatively large ice particles, the 89- and 150-GHz channels are important tools for D_e and IWP retrievals. Because different particle sizes may produce similar radiance patterns using a single frequency, this dual-frequency technique reduces the ambiguity in the relationship between radiance and particle size (Weng and Grody 2000). However, uncertainties related with ice density and cloud base brightness temperature estimates could affect these retrievals (Sun and Weng 2012).

Tropical convective clouds could be examined using cloud-top temperature information. The thermal infrared channel (10.8 μm) from geostationary satellites is used to extract the morphological characteristics and radiative properties of these clouds. Machado and Rossow (1993) and Machado et al. (1998) provide a detailed analysis of cloud life cycle climatology for mesoscale convective systems (MCSs) over the Americas. Wang et al. (1997) found that the use of water vapor absorption channels (183 GHz) from passive

Corresponding author address: Ramon Campos Braga, PTEC/INPE, Rod. Pres. Dutra km 40, Cachoeira Paulista, São Paulo 12630-000, Brazil.
E-mail: ramon.braga@cptec.inpe.br

DOI: 10.1175/JHM-D-13-0206.1

microwave sensors could also provide convective cloud information.

Ground radar is also an important tool for convection analysis (Steiner et al. 1995; Awaka et al. 1998). The cloud classification method proposed by Steiner et al. (1995) uses radar reflectivities at a specific altitude [constant altitude plan position indicator (CAPPI)] to discriminate convective and stratiform cloud structures. The altitude closest to the cloud base is considered (2 km in midlatitude case and 3 km in tropical case). Although this method has shown some efficiency in classifying clouds as convective or stratiform, errors can be found for different precipitating systems and because of inherent radar observational deficiencies at longer ranges (Biggerstaff and Listermaa 2000; Gorgucci et al. 2006).

The main objectives of this study are to analyze the relationship between IWP retrievals using satellites and the life cycle stage of convective clouds and the possible applications for satellite-based rain rate retrievals. In the first part of this work, the relationship between IWP and the cloud area expansion rate is analyzed using the 235-K isotherm. The IWP is retrieved using the Microwave Surface and Precipitation Products System (MSPPS), which uses high-frequency channels (89 and 150 GHz) from the Advanced Microwave Sounding Unit-B (AMSU-B) and Microwave Humidity Sounder (MHS) sensors on board National Oceanic and Atmospheric Administration (NOAA) satellites (*NOAA-16–NOAA-19*). Moreover, the cloud expansion rate was calculated using the Forecast and Tracking the Evolution of Cloud Clusters (ForTraCC) algorithm (Vila et al. 2008), which identifies and tracks the evolution of mesoscale convective systems from geostationary satellite thermal infrared images (10.7 μm). In the second step, the relationship of cloud convective fraction with rain rates (using radar data) and with the cloud life cycles were analyzed. This research is part of the Brazilian contribution to the Global Precipitation Measurement (GPM) project (GPM-Brazil) for precipitating events, which occurred during the Cloud Processes of the Main Precipitation Systems in Brazil: A Contribution to Cloud Resolving Modeling and to the Global Precipitation Measurement (CHUVA) experiment at Vale do Paraíba.

2. Region of study

The region of study is the area covered by the X-band radar from the CHUVA project at São José dos Campos (SJC; 23.2°S, 45.95°W) during the period from November 2011 to March 2012 (see location in Fig. 1). The region is affected primarily by cold fronts, the South Atlantic convergence zone (SACZ; Satyamurty et al. 2008), and thermally induced convection due to surface heating. The period coincides with the 2011/12 rainy season.

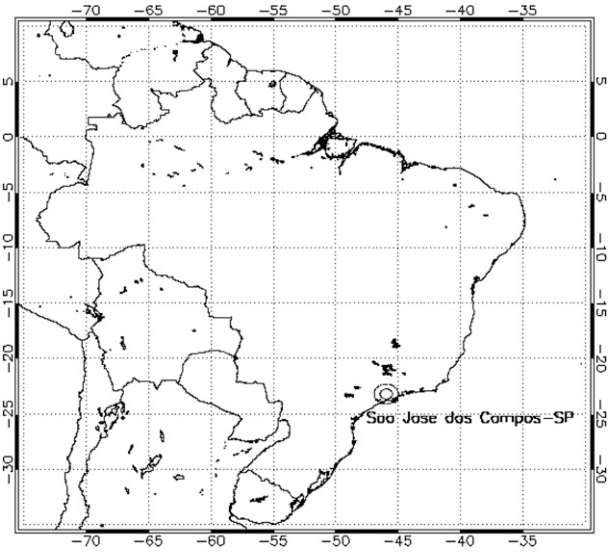

FIG. 1. Area covered by the radar in SJC.

3. Database

a. *Satellite data*

1) NOAA DATA

The MSPPS (Ferraro et al. 2005), which was used for IWP, D_e, and rain rate RR retrievals, uses information from high-frequency channels (89 and 150 GHz for AMSU-B; 89 and 157 GHz for MHS) from AMSU-B and MHS (*NOAA-16–NOAA-19*). The AMSU-B and MHS sensors operate in a cross-track scan with a spatial resolution near 16 km at nadir view (Bennartz 2000). Only pixels with a viewing angle less than ±30° were used to avoid large pixel deformation and viewing angle dependencies.

The IWP was calculated as a function of D_e, θ, and ρ. The retrieval algorithms were developed and tested using aircraft millimeter-wavelength measurements (Weng and Grody 2000).

The rain rate estimation algorithm using AMSU-B/MHS sensors over land was based on ice scattering measurements using microwave-band high-frequency information, that is, 89 and 150/157 GHz (Ferraro et al. 2005). Additionally, the water vapor channels (183 ± 1 GHz, 183 ± 3 GHz, and 183 ± 7 GHz) were used to analyze the cloud convection environment and determine which empirical rain rate equation should be used (different equations were used for weak or moderate and heavy rain).

2) *GOES-12* DATA

The life cycle information was extracted from the operational version of the ForTraCC algorithm (Vila et al. 2008), which uses information from *Geostationary Operational Environmental Satellite-12* (*GOES-12*; channel 4) to identify and track convective clouds with brightness temperature below 235 K.

The life cycle information was obtained from the ForTraCC output. Three life cycle stages were considered: 1) intensifying, when the MCS area is growing and the minimum brightness temperature TB_{min} is decreasing; 2) dissipating, when the MCS area variation is either zero or negative or TB_{min} is increasing; and 3) not identified, when ForTraCC does not identify the MCS and the IWP is greater than zero (according to MSPPS). The operational version of ForTraCC used in the present study uses a size threshold of 1440 km^2; the cloud system identification is based on a 235-K temperature threshold.

b. Radar data

An X-band dual-polarization radar, which has a horizontal and vertical grid resolution of 0.25 km, was used during the CHUVA–Geostationary Lightning Mapper (GLM) project at Vale do Paraíba as the data source for the reflectivity Z, rain radar rate RR_x (Bringi et al. 2007), and cloud hydrometeor (Keenan 2003). Although X-band radars have been widely used in contemporary rainfall estimates, the attenuation is larger than in S- and C-band radars (Gorgucci et al. 2006). To reduce these limitations, the specific differential propagation phase K_{dp} was used instead of the reflectivity–rainfall (Z–R) relation to attain more accurate retrievals (Gorgucci et al. 2006).

The CAPPI at 2 km was used for cloud classification and precipitation retrieval. The radar range was limited to 60 km for the X-band radar. To take advantage of the X-band radar polarimetric variables from São José dos Campos, the following equation is used (Bringi et al. 2007):

$$Z = \begin{cases} \text{for} \quad Z < 35 \quad \text{and} \quad K_{dp} \le 0.3 \text{ uses } Z = 200 RR_x^{1.6} \\ \text{for} \quad Z \ge 35 \quad \text{and} \quad K_{dp} > 0.3 \text{ uses } RR_x = 19.63 |K_{dp}|^{0.823}. \end{cases} \tag{1}$$

Here, Z is the horizontal reflectivity, RR_x is the radar rain rate, and K_{dp} is the specific differential phase. Large K_{dp} values ($K_{dp} > 2^\circ\,km^{-1}$) suggest the presence of large amounts of liquid water and/or highly oriented (i.e., oblate) shapes. Moreover, K_{dp} is a very good estimator for rainfall because the attenuation caused by heavy rain is largely reduced (Bringi et al. 2007).

The convective fraction and rain rate related to each AMSU-B or MHS pixel were only considered in cases where pixels had at least 70% of the radar coverage to avoid statistical inconsistencies. The reflectivity horizontal distribution at a specific altitude near cloud base (2 km in this case) is used to classify cloud as either convective or stratiform (Steiner et al. 1995).

4. Methodology

The analysis was performed in three steps. In the first step, *NOAA-16–NOAA-19* passages were superimposed with radar areas during the studied period. A maximum time interval of 2 min between the radar and satellite measurements was considered. The maximum time interval for tracking information is 7 min because the information is available only every 15 min (*GOES-12* over South America). During the studied period, 413 NOAA satellite passages over the SJC region met these requirements. From all passages, 87 precipitating events were observed over SJC. Considering the AMSU-B/MHS spatial resolution (~16 km at nadir) and the size of the analyzed storms, 376 AMSU-B/MHS pixels were analyzed.

After the selection process, a cloud classification algorithm (convective or stratiform) was applied using radar reflectivity data (Steiner et al. 1995). Then, the IWP and effective ice particle diameter statistical parameters from the MSPPS were calculated as a function of convective fraction and cloud life cycle.

Finally, the MSPPS RR estimates were analyzed for precipitating events. Based on these results, a new set of rainfall rate retrieval equations was tested using D_e and IWP data. The rain rates using the newly proposed equations were compared with the current MSPPS methodology.

5. Results and discussion

a. IWP analysis and cloud life cycle

To closely analyze the behavior of all examined parameters for a specific case, the variables were analyzed for a convective system over SJC on 8 January 2012 (Figs. 2a–d). According to the ForTraCC algorithm, this event is in the intensification stage because its area is expanding [$\Delta A/\Delta t \sim 3800\,km^2\,(30\,min)^{-1}$] and its minimum brightness temperature is decreasing [$\Delta T/\Delta t \sim 8^\circ C\,(30\,min)^{-1}$]. The IWP retrieved with the MSPPS algorithm is approximately $1\,kg\,m^{-2}$ (Fig. 2a) in the maximum rain rate area, that is, greater than $40\,mm\,h^{-1}$

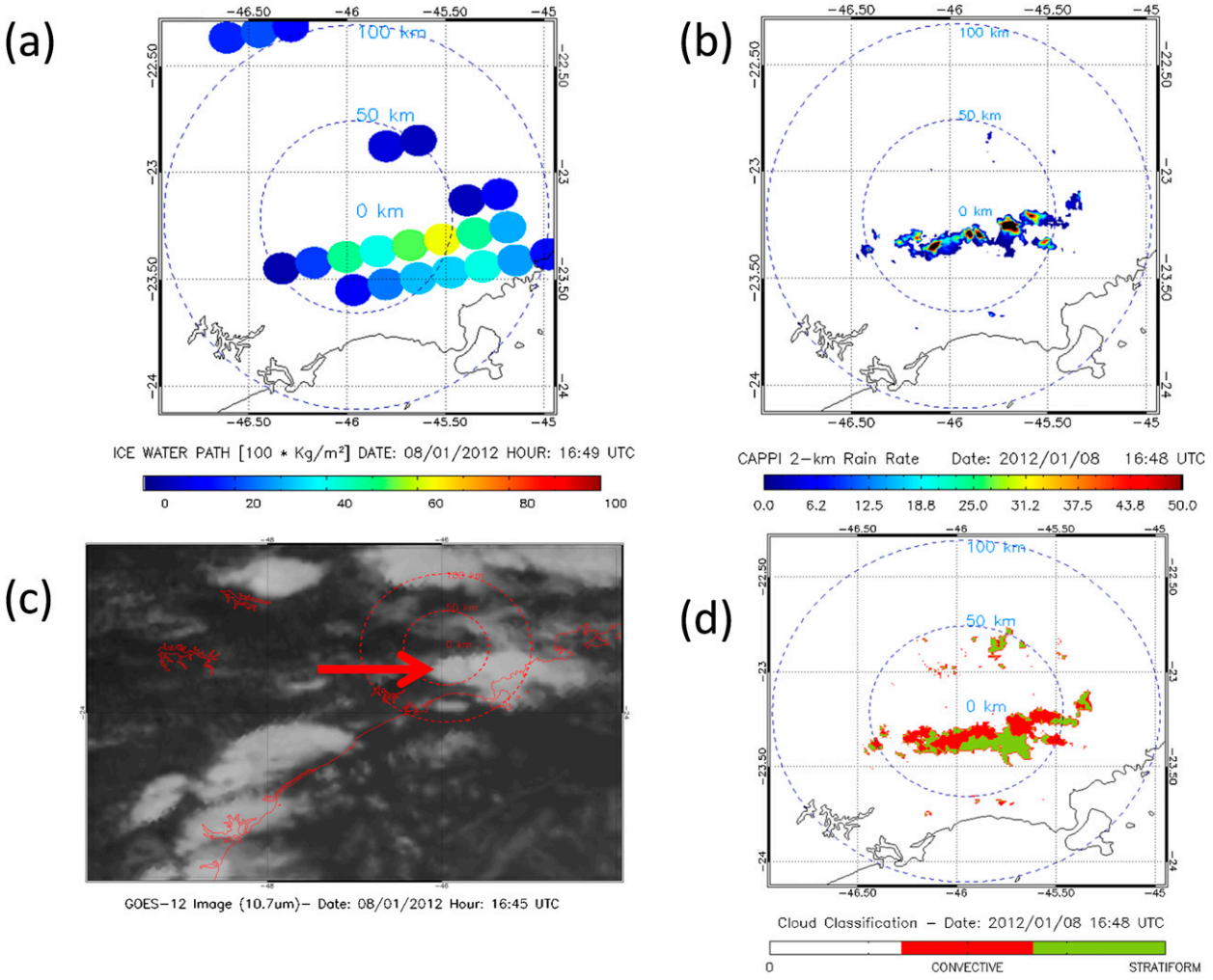

FIG. 2. (a) IWP (100 kg m^{-2}) inferred with the MSPPS algorithm, (b) RR$_x$, (c) *GOES-12* image (10.7 μm) for the precipitating event at 1645 UTC 8 Jan 2012, and (d) convective/stratiform cloud classification. The red arrow indicates the event in (c).

(Fig. 2b). Figure 2c shows the *GOES-12* 10.7-μm image; the observed system is indicated with a red arrow. The cloud classification scheme (Fig. 2d) shows that the most active region of the system is classified as convective. This case study suggests that MCSs with large IWPs tend to be classified as convective during the intensification stage. An extensive statistical analysis, performed to verify (or not) this hypothesis and to determine the circumstances for which it is valid, is provided below.

Figure 3 shows the IWP frequency histogram for the identified and unidentified pixels according to ForTraCC over the SJC region. In total, 23% of the clouds are in the intensification stage, and 21% of the clouds are in the dissipating stage. For the cases where ForTraCC could not identify a system (according to the thresholds used in this study), 40% have ice (according to the MSPPS) and 16% are from warm precipitating clouds. Therefore, ice is detected in 84% of the precipitating clouds using the MSPPS algorithm near SJC and 16% of the clouds contain only liquid water. For clouds containing ice, 54% are identified with ForTraCC; the other 46% are not identified. In a closer analysis (not shown), most systems containing ice and not identified by ForTraCC occur in clouds with cloud-top brightness temperatures greater than 235 K and less than the freezing point.

Figure 4a shows the IWP behavior as a function of cloud life cycle over the SJC area. The central box is the interquartile extent (Q3–Q1); the central line is the sample median. The maximum and minimum values and outliers are also shown. When clouds are in the intensification (INT) stage, the IWP scatter diagram is displaced toward larger values than in the dissipating (DIS) stage. A less scattered graph with a lower median is observed in ice clouds not identified by ForTraCC (NID). The same behavior is verified for radar-estimated

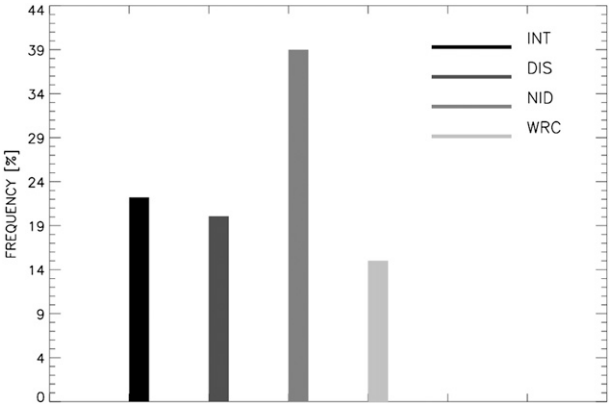

FIG. 3. Frequency histogram for the 376 AMSU-B/MHS pixels from *NOAA-16–NOAA-19* passages over SJC. The shade indicates the observed classes according to ForTraCC: INT, DIS, NID, and WRC.

rain rates (i.e., RR_x) as a function of cloud life cycle (see Fig. 4b). The rain rate in warm clouds (WRC), that is, clouds with no ice, according to the MSPPS, is less than the rain rate in the previously mentioned stages.

Furthermore, D_e slightly varies as a function of cloud life cycle (Fig. 4c). The D_e distribution is nearly the same for all life cycle stages, even for DIS and NID, which are associated with lower IWPs (Fig. 4a). A possible explanation for this result is that in the DIS and NID stages, the ice particles are a mixture of air and ice, which reduces the ice density (lower IWP) while the D_e could increase via aggregation. However, more in situ observations are needed to study the microphysical nature of these types of precipitation events.

The radar-observed cloud convective fraction for AMSU-B/MHS pixels is presented in Fig. 4d, demonstrating that the convective fraction and IWP distributions are similar. Specifically, larger cloud convective fractions are found in the INT stage than in the DIS stage. Moreover, smaller convective fractions are found in warm clouds or clouds with low ice content.

To investigate the small variation in D_e inferred by AMSU-B/MHS sensors during the cloud life cycle, two case studies were chosen to show the IWP and D_e variations in different cloud life cycle stages (i.e., intensifying and dissipating). Figures 5a–c show the IWP and D_e inferred with the MSPPS methodology and the X-band radar rain rate at 2324 UTC 15 January 2012. This system is intensifying according to ForTraCC. In this case, large IWP ($\sim 1.2\,kg\,m^{-2}$) and D_e (~ 2 mm) values are observed in the most intense storm regions (i.e., where $RR_x > 50\,mm\,h^{-1}$). A vertical cross section of the hydrometeor classification using the dual-polarization radar in the two most intense storm regions (indicated in Figs. 5a–c as segments A–B and C–D) are shown in Figs. 6a and 6b. A hail and rain mixture is observed for

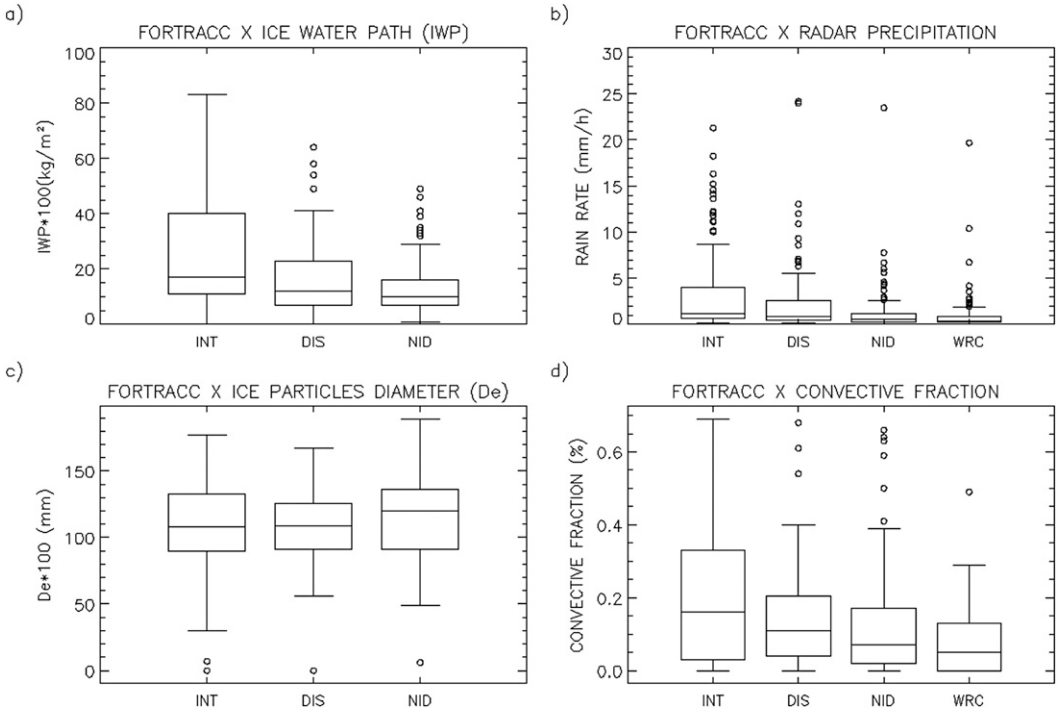

FIG. 4. Box-and-whisker plot for (a) IWP, (b) RR_x, (c) D_e, and (d) convective fraction as a function of the cloud life cycle. The observations are the same as in Fig. 3.

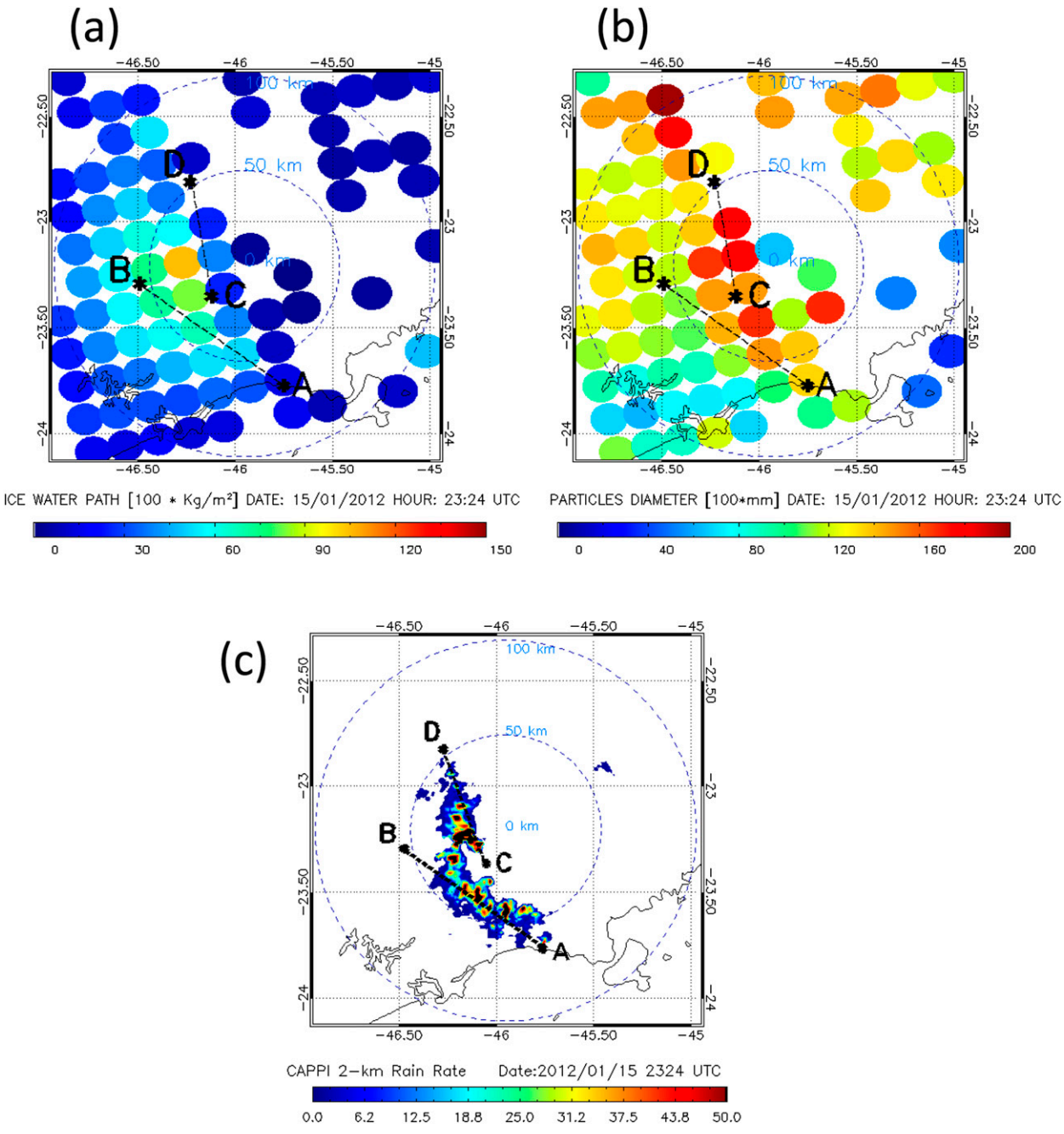

FIG. 5. (a) IWP inferred with the MSPPS, (b) D_e inferred with the MSPPS, and (c) RR_x from CAPPI at 2 km for a cloud in the intensifying stage. Segments A–B and C–D indicate the hydrometeor radar cross sections shown in Figs. 6a and 6b.

segment A–B, while a deep rainfall layer is observed in segment C–D. The other case represents a dissipating convective cloud. Figures 7a–c show the same analysis as in Figs. 5a–c, but at 0418 UTC 10 December 2011. Smaller IWP ($\sim 0.3\,kg\,m^{-2}$), D_e ($\sim 1\,mm$), and RR_x ($\sim 10\,mm\,h^{-1}$) values are observed in this case than for the intensifying stage (Figs. 7a–c). The vertical cross section of the hydrometeor classification (indicated in Figs. 7a–c as segment A–B) is shown in Fig. 8. Here, graupel and wet snow, typically formed by aggregation in dissipating clouds, and rain at the surface are observed. Moreover, the convective system height is substantially lower at this stage than in the intensifying stage. Although the D_e values are lower in the dissipating stage than in the intensifying stage, the values are not negligible, suggesting that the MSPPS is sensitive to the ice

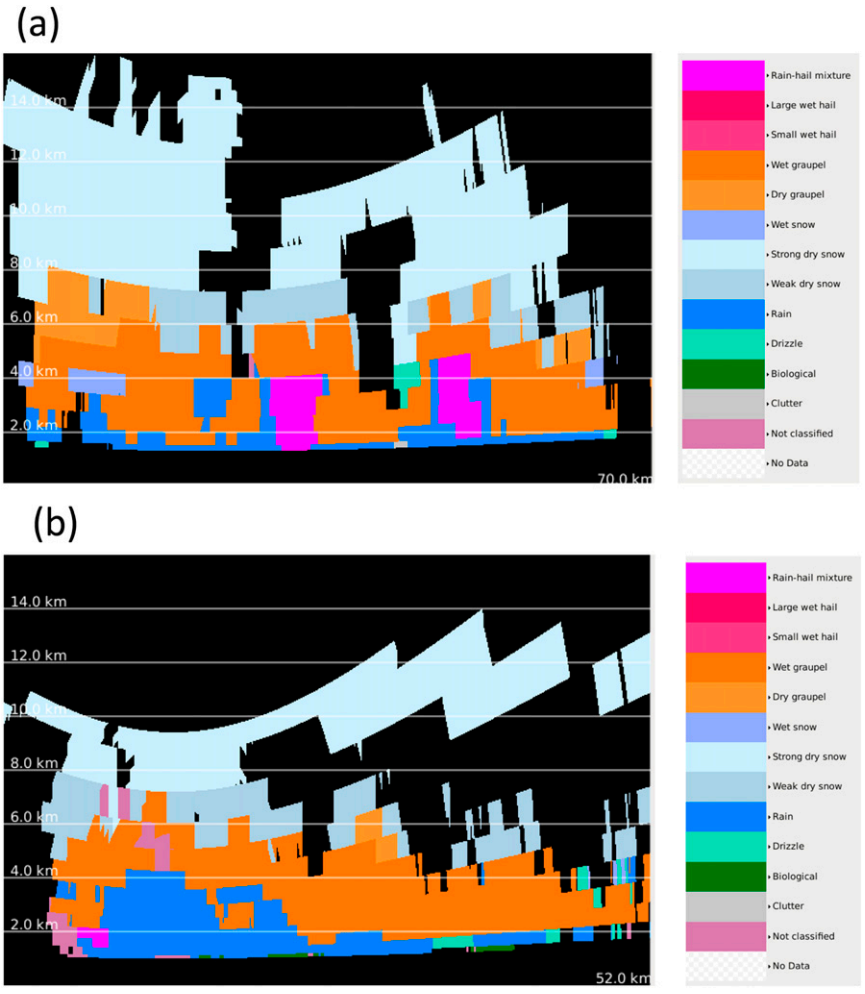

FIG. 6. Vertical hydrometeor classification radar cross section from Figs. 5a–c. (a) Segment A–B (A indicates the left side and B indicates the right side) and (b) segment C–D (C indicates the left side and D indicates the right side).

type observed in this stage. These findings are in accordance with Fig. 4c.

According to the hydrometeor cross sections, MSPPS-detected D_e and IWP could provide cloud life cycle and ice particle type and size information. These observed patterns are investigated in the following section; a new set of rainfall retrieval equations is proposed.

b. *MSPPS rain rate estimate analysis*

A new set of rain rate retrieval equations was tested for the SJC region using IWP and D_e information. This new methodology is based on the IWP and D_e results from the previous section, cloud life cycle characteristics (inferred with microwave frequencies), and recent studies related to lightning in thunderstorms. Mattos and Machado (2011) found that for D_e larger than 1.2 mm (also inferred with the MSPPS algorithm), the lightning probability is higher than for smaller particles. Consequently, greater convection is observed. The observations of Wang et al. (2012) also support the close relationship between convection and lightning.

An analysis of the IWP versus RR_x distribution for high ($D_e > 1.2$ mm) and low ($D_e < 1.2$ mm) lightning probabilities is shown in Fig. 9, demonstrating that RR_x tends to be higher for nearly all IWP ranges in most cases when D_e is larger than 1.2 mm. Moreover, for small particles, the observed rain rates are quite small even with large IWP values. The formation of large ice particles (with diameters larger than 0.4 mm) occurs primarily in cloud layers with temperatures between 0° and −30°C (Liu and Curry 1998) via riming or aggregation. The ice size is an indication of precipitating clouds. However, this characteristic of cloud composition is not sufficient to provide structural and cloud dynamic stage information.

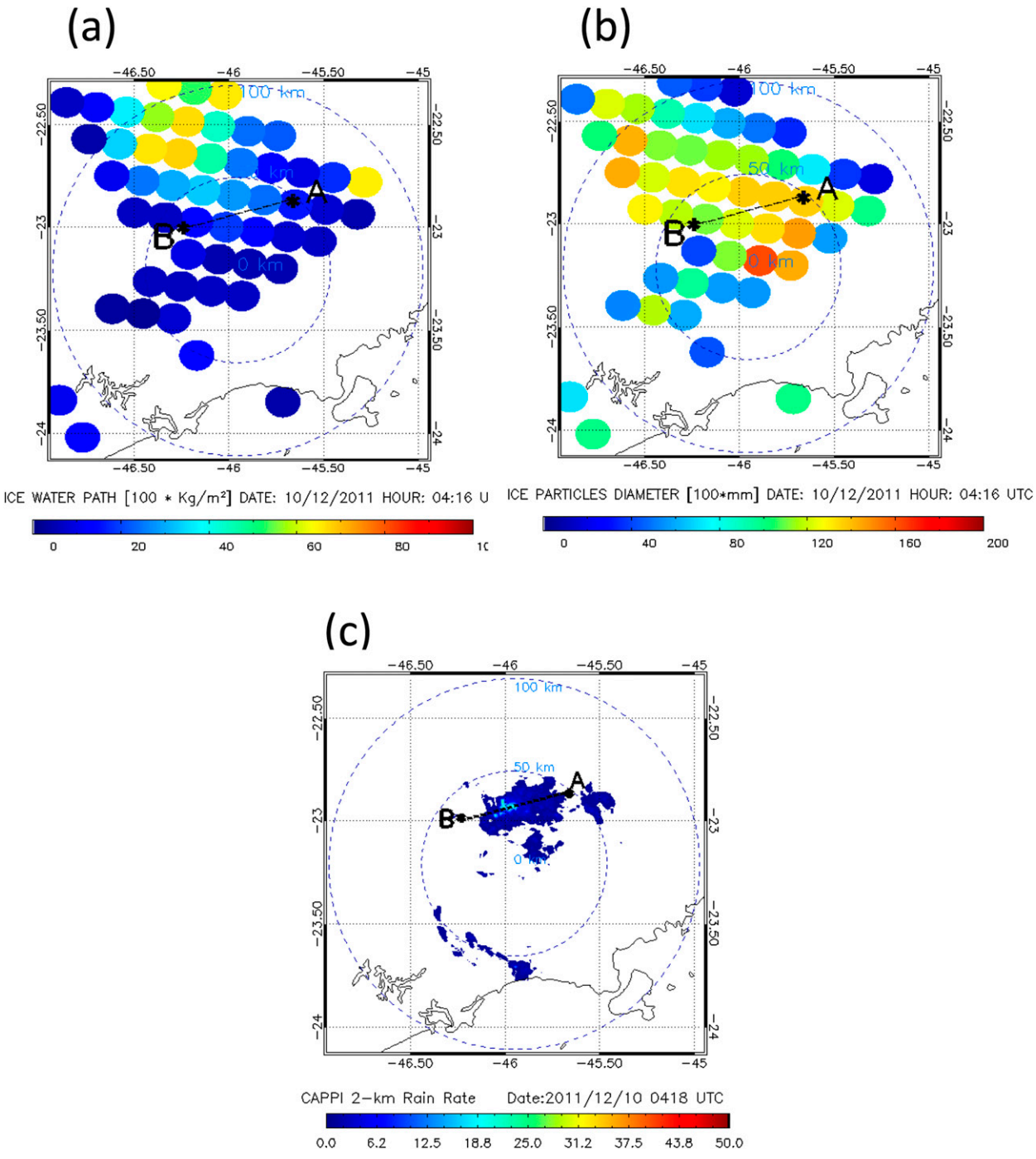

FIG. 7. (a) IWP inferred with the MSPPS, (b) D_e inferred with the MSPPS, and (c) RR_x from CAPPI at 2 km for a cloud in the dissipating stage. Segment A–B indicates the hydrometeor radar cross section shown in Fig. 8.

Based on our findings, a new methodology for rain rate estimation using IWP values (which provide life cycle information) for different D_e ranges (which suggest strong convection for values larger than 1.2 mm) is proposed.

For validation purposes, the entire dataset for SJC (376 pixels that belong to 87 different events) were randomly separated: ~70% of the data (263 AMSU/MHS pixels) were used for the methodology development (training data); the remaining data (113 AMSU/MHS

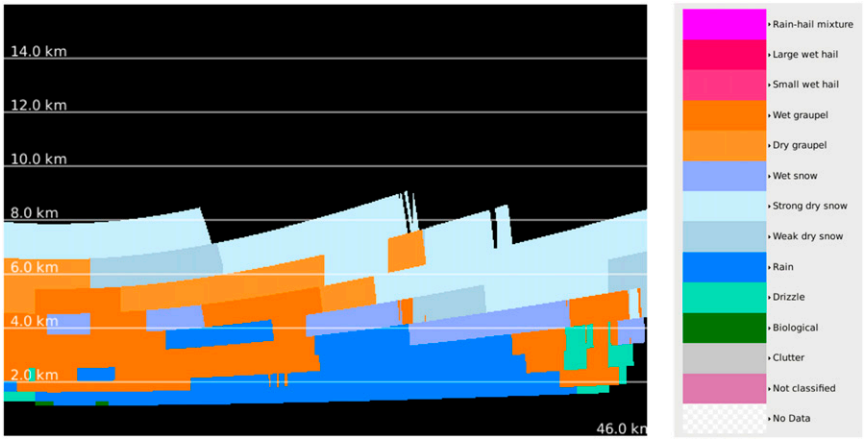

FIG. 8. Vertical hydrometeor classification radar cross section from Figs. 7a–c. Segment A–B (A indicates the left side and B indicates the right side).

pixels) were used for validation (validating data). For D_e less than 0.4 mm, the cloud is considered an anvil or cirrus cloud (i.e., nonprecipitating cloud). The 0.4-mm threshold was determined using the minimum box plot value in the training data (figure not shown). For D_e larger than 1.2 mm, the rainfall rates may be higher than for smaller particles because of their relationship with the convective environment. If the size is between 0.4 and 1.2 mm, light rain rate may be observed. The rain rate spatial scale is based on the AMSU-B/MHS pixel size (~16 km), which could weaken high rain rates from strong local convection in the data. The D_e-stratified rain rate data are shown in Fig. 10 for the training data.

Based on the previous analyses, new empirical equations were developed with the training data for the SJC area. After a fitting process, a linear rain rate estimation equation was determined because it provided a better correlation coefficient and lower standard deviation compared with other fitting functions (e.g., parabolic and exponential). The equations are as follows:

$$\text{if} \quad D_e \le 0.4\,\text{mm}; \quad \text{RR} = 0\,\text{mm h}^{-1}, \tag{2}$$

$$\text{if} \quad 0.4 < D_e < 1.2\,\text{mm}; \quad \text{RR} = 1.38(\text{IWP}) + 0.9953, \tag{3}$$

and

$$\text{if} \quad D_e \ge 1.2\,\text{mm}; \quad \text{RR} = 20.64(\text{IWP}) - 0.5237. \tag{4}$$

Table 1 presents the statistical parameters [i.e., linear correlation (COR), bias, probability of detection

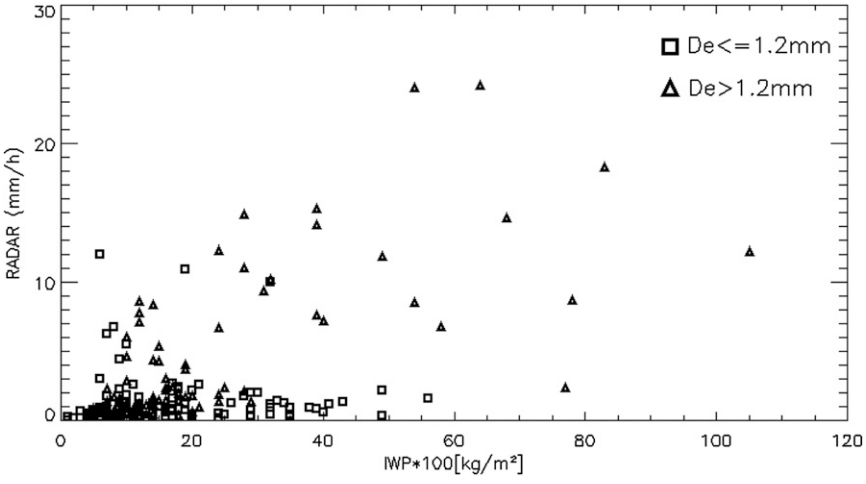

FIG. 9. RR_x (RADAR) as a function of the IWP over the SJC region. The squares are related to cases with $D_e \le 1.2$ mm and triangles correspond to diameters >1.2 mm.

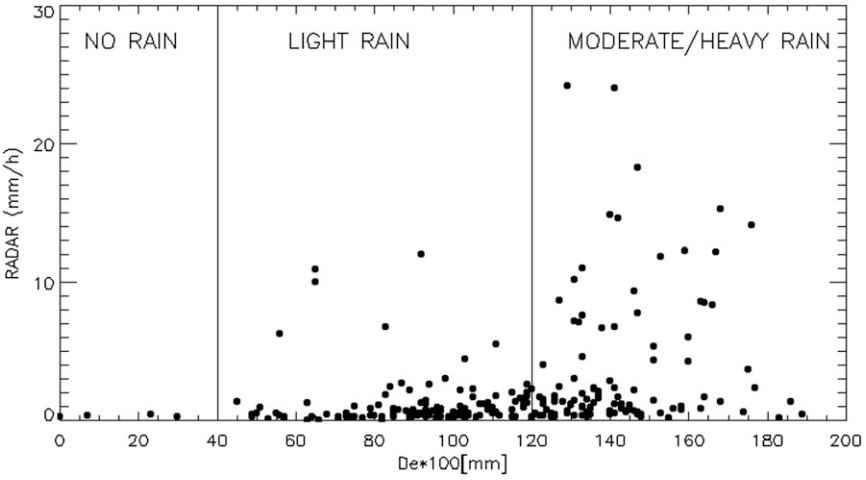

FIG. 10. RR_x (RADAR) as a function of D_e over the SJC region. The rain rate regions are divided into different D_e ranges as proposed by the new methodology.

(POD), false alarm ratio (FAR), and root-mean-square error (RMSE)] for a comparison between the proposed method (PRED_IWP) and the actual data from the MSPPS algorithm (MSPPS) using the validation data pixels over the SJC region. These preliminary results, based on a limited dataset during the CHUVA-GLM campaign, show a substantial improvement compared with the MSPPS global model. A better agreement is also found using the new method for the accumulated rainfall and PDF distributions (Table 2, Fig. 11).

The IWP and D_e information provide important information about storm characteristics, which show improvement in the rain rate retrieval using the MSPPS algorithm. The current MSPPS global version rain rate retrieval, which uses a convective index derived from the water vapor channels, performed worse than the new rain rate retrieval. The reason for this result could be due to the new method use regional training data, and it is also validated in the same region. However, it is important to observe that the new methodology could classify better convective and stratiform clouds, associated to the cloud life cycle, than the current convective index. This could lead to an improvement of the rain rate retrieval for the study region.

TABLE 1. Statistics for validating data using the MSPPS algorithm and PRED_IWP.

Model	COR	Bias	POD	FAR	RMSE
MSPPS	0.28	1.82	0.94	0.69	4.22
PRED_IWP	0.53	0.28	0.97	0.68	3.13

6. Conclusions

The objectives of the present study are to describe the IWP behavior as a function of cloud life cycle over São José dos Campos (SJC) during the rainy season and to investigate the possible use of this information to improve microwave-based rainfall rate estimates inferred by satellites. The results showed that in SJC, rainfall is primarily caused by ice clouds (84%) according to the MSPPS algorithm. During the first stages of the cloud life cycle (INT), larger values of IWP, RR_x, and convective fraction are observed than in the dissipation stage (DIS). Moreover, D_e does not exhibit large variations as a function of the cloud life cycle. To investigate this behavior, two case studies were analyzed to determine the IWP and D_e variations in different cloud life cycle stages (intensifying and dissipating). The results suggest that the combination of D_e and IWP data could provide cloud life cycle information, because higher IWP and D_e values are observed in intensifying systems; lower IWP and relatively large D_e values are observed in the dissipating stage. The newly proposed methodology for rain rate retrieval by including cloud life cycle patterns for IWP and D_e substantially improved the predictions compared with the global algorithm developed for the MSPPS. Future work is

TABLE 2. Rain rates accumulated for validating data from the X-band radar, MSPPS, and PRED_IWP.

Models	Accumulated RR ($mm\,h^{-1}$)
RADAR	219.63
MSPPS	437.8
PRED_IWP	253.55

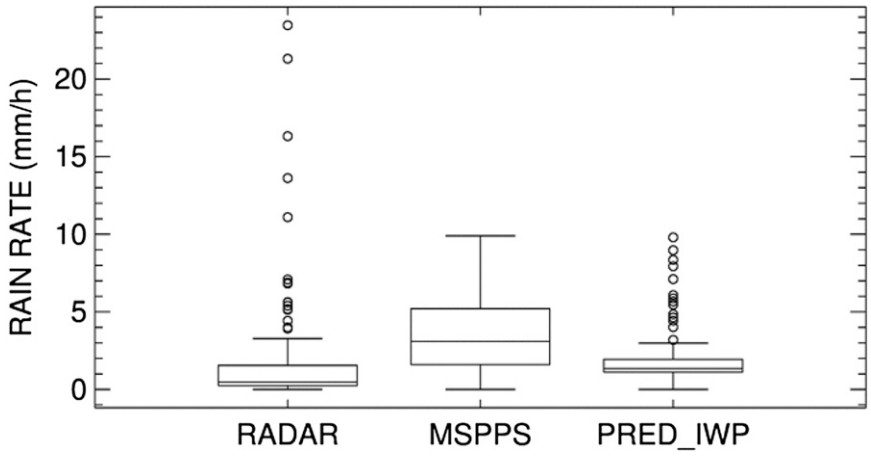

FIG. 11. Box-and-whisker plot for the RR_x (RADAR), MSPPS algorithm, and the new methodology (PRED_IWP) proposed for validating data.

needed to further validate this new methodology using a larger and more comprehensive database that considers different rainfall regimes. The inclusion of life cycle information could also help improve satellite-based rain rate retrievals. Furthermore, future comparative studies with other precipitation estimates using satellite data are needed.

Acknowledgments. The authors acknowledge the Center for Weather Forecast and Climate Studies, the National Institute for Space and Research (CPTEC/INPE) and the CHUVA project (FAPESP Grant 2009/15235-8) for the data and infrastructure for the development of this research. The first author also acknowledges the financial support of the Brazilian National Science Council (CNPq) during his master's degree studies. Both authors also thank Thiago Biscaro for the radar data support.

REFERENCES

Awaka, J., T. Iguchi, and K. Okamoto, 1998: Early results on rain type classification by the Tropical Rainfall Measuring Mission (TRMM) precipitation radar. *Proc. 8th URSI Commission F Triennial Open Symp.,* Aveiro, Portugal, URSI, 143–146.

Bennartz, R., 2000: Optimal convolution of AMSU-B to AMSU-A. *J. Atmos. Oceanic Technol.,* **17,** 1215–1225, doi:10.1175/1520-0426(2000)017<1215:OCOABT>2.0.CO;2.

Biggerstaff, M., and S. Listermaa, 2000: An improved scheme for convective/stratiform echo classification using radar reflectivity. *J. Appl. Meteor.,* **39,** 2129–2150, doi:10.1175/1520-0450(2001)040<2129:AISFCS>2.0.CO;2.

Bringi, V. N., M. Thurai, and R. Hannesen, Eds., 2007: Hydrometeor classification at S, C and X-bands. *Dual-Polarization Weather Radar Handbook,* 2nd ed. Gematronik, 163 pp.

Ferraro, R., and Coauthors, 2005: NOAA operational hydrological products derived from the Advanced Microwave Sounding Unit (AMSU). *IEEE Trans. Geosci. Remote Sens.,* **43,** 1036–1049, doi:10.1109/TGRS.2004.843249.

Gorgucci, E., V. Chandrasekar, and L. Baldini, 2006: Correction of X-band radar observation for propagation effects based on the self-consistency principle. *J. Atmos. Oceanic Technol.,* **23,** 1668–1681, doi:10.1175/JTECH1950.1.

Keenan, T. D., 2003: Hydrometeor classification with a C-band polarimetric radar. *Aust. Meteor. Mag.,* **52,** 23–31.

Liu, G., and J. A. Curry, 1998: Remote sensing of ice water characteristics in tropical clouds using aircraft microwave measurements. *J. Appl. Meteor.,* **37,** 337–355, doi:10.1175/1520-0450(1998)037<0337:RSOIWC>2.0.CO;2.

Machado, L. A. T., and W. B. Rossow, 1993: Structural characteristics and radiative properties of tropical cloud clusters. *Mon. Wea. Rev.,* **121,** 3234–3260, doi:10.1175/1520-0493(1993)121<3234:SCARPO>2.0.CO;2.

——, ——, R. L. Guedes, and A. W. Walker, 1998: Life cycle variations of mesoscale convective systems over the Americas. *Mon. Wea. Rev.,* **126,** 1630–1654, doi:10.1175/1520-0493(1998)126<1630:LCVOMC>2.0.CO;2.

Mattos, E. V., and L. A. T. Machado, 2011: Cloud-to-ground lightning and mesoscale convective systems. *Atmos. Res.,* **99,** 377–399, doi:10.1016/j.atmosres.2010.11.007.

Rossow, W. B., and R. A. Schiffer, 1991: ISCCP cloud data products. *Bull. Amer. Meteor. Soc.,* **72,** 2–20, doi:10.1175/1520-0477(1991)072<0002:ICDP>2.0.CO;2.

——, and ——, 1999: Advances in understanding clouds from ISCCP. *Bull. Amer. Meteor. Soc.,* **80,** 2261–2288, doi:10.1175/1520-0477(1999)080<2261:AIUCFI>2.0.CO;2.

Satyamurty, P., S. S. B. Junior, M. S. Teixeira, and L. E. M. G. Silva, 2008: Regional circulation differences between a rainy episode and a nonrainy episode in eastern São Paulo state in March 2006. *Rev. Bras. Meteor.,* **23,** 404–416, doi:10.1590/S0102-77862008000400003.

Steiner, M., R. A. Houze Jr., and S. R. Yuter, 1995: Climatological characterization of three-dimensional storm structure from operational radar and rain gauge data. *J. Appl. Meteor.,* **34,** 1978–2007, doi:10.1175/1520-0450(1995)034<1978:CCOTDS>2.0.CO;2.

Sun, N., and F. Weng, 2012: Retrieval of ice water path from Special Sensor Microwave Imager/Sounder (SSMIS). *J. Appl. Meteor. Climatol.,* **51,** 366–379, doi:10.1175/JAMC-D-11-021.1.

Vila, D. A., L. A. T. Machado, H. Laurent, and I. Velasco, 2008: Forecast and Tracking the Evolution of Cloud Clusters (ForTraCC) using satellite infrared imagery: Methodology and validation. *Wea. Forecasting,* **23,** 233–245, doi:10.1175/2007WAF2006121.1.

Vivekanandan, J., J. Turk, and V. N. Bringi, 1991: Ice water path estimation and characterization using passive microwave radiometry. *J. Appl. Meteor.,* **30,** 1407–1421, doi:10.1175/1520-0450(1991)030<1407:IWPEAC>2.0.CO;2.

Wang, J. R., J. Zhan, and P. Pacette, 1997: Storm-associated microwave radiometric signatures in the frequency range of 90–220 GHz. *J. Atmos. Oceanic Technol.,* **14,** 13–31, doi:10.1175/1520-0426(1997)014<0013:SAMRSI>2.0.CO;2.

Wang, N., K. Gopalan, and R. I. Albrecht, 2012: Application of lightning to passive microwave convective and stratiform partitioning in passive microwave rainfall retrieval algorithm over land from TRMM. *J. Geophys. Res.,* **117,** D23203, doi:10.1029/2012JD017812.

Weng, F., and N. C. Grody, 2000: Retrieval of ice cloud parameters using microwave imaging radiometer. *J. Atmos. Sci.,* **57,** 1069–1081, doi:10.1175/1520-0469(2000)057<1069:ROICPU>2.0.CO;2.